Supplemental Material for "Error-Tolerant Amplification and Simulation of the Ultrastrong-Coupling Quantum Rabi Model"

Ye-Hong Chen,[1,2,3] Zhi-Cheng Shi,[1,2] Franco Nori,[3,4,5] and Yan Xia[1,2,*]

[1] *Fujian Key Laboratory of Quantum Information and Quantum Optics, Fuzhou University, Fuzhou 350116, China*
[2] *Department of Physics, Fuzhou University, Fuzhou 350116, China*
[3] *Theoretical Quantum Physics Laboratory, RIKEN Cluster for Pioneering Research, Wako-shi, Saitama 351-0198, Japan*
[4] *Quantum Information Physics Theory Research Team, RIKEN Center for Quantum Computing, Wako-shi, Saitama 351-0198, Japan*
[5] *Department of Physics, University of Michigan, Ann Arbor, Michigan 48109-1040, USA*

(Dated: May 31, 2024)

S1. POSSIBLE IMPLEMENTATION WITH SUPERCONDUCTING CIRCUITS

Kerr-cat qubits have been experimentally realized in superconducting circuits [S1, S2]. Using the same physical setup with that in Ref. [S1], a circuit diagram for implementing our protocol is shown in Fig. S1(a). We consider that a transmission-line resonator (i.e., LC resonator) is coupled to an array of N Josephson junctions with Josephson energy $E_J[\Phi(t)] = E_J - \delta E_J \cos\omega_p t$, which depends on a harmonically modulable external flux $\Phi(t)$ with modulation frequency ω_p. Following the standard quantization procedure for circuits [S3, S4], the Hamiltonian for the system is (hereafter $\hbar = 1$):

$$\begin{aligned}
H_{\rm tot} =& H_{LC} + H_{\rm KNR}^{(0)} + H_{\rm int},\\
H_{LC} =& \omega a^\dagger a,\\
H_{\rm KNR}^{(0)} =& 4E_C\hat{n}^2 - NE_J[\Phi(t)]\cos\frac{\hat{\phi}}{N},\\
H_{\rm int} =& n_0\lambda(a^\dagger + a)\hat{n}.
\end{aligned} \tag{S1}$$

Here, $\omega = 1/\sqrt{L_rC_r}$ and a ($a^\dagger$) are the frequency and the annihilation (creation) operator of the LC resonator, respectively; $\hat{n}$ and $\hat{\phi}$ are the number of the Cooper pairs and the overall phase across the junction array, respectively; E_C is the charging energy and $\lambda = 2C_g e\sqrt{\omega/2C_r}/(C_g + C_B)$ is the coupling strength. Then, by introducing the definitions $\hat{n} = -in_0(b - b^\dagger)$ and $\hat{\phi} = \phi_0(b + b^\dagger)$, the quadratic time-independent part of the Hamiltonian $H_{\rm KNR}$ can be diagonalized, where n_0 and ϕ_0 are zero-point fluctuations [S1].

Focusing on the Hamiltonian $H_{\rm KNR}$, we have

$$\begin{aligned}
H_{\rm KNR}^{(0)} =& 4E_C\hat{n}^2 - NE_J\left[1 - \frac{1}{2}\left(\frac{\hat{\phi}}{2}\right)^2 + \frac{1}{24}\left(\frac{\hat{\phi}}{2}\right)^4 + \cdots\right] - N\delta E_J\left[1 - \frac{1}{2}\left(\frac{\hat{\phi}}{2}\right)^2 + \cdots\right]\cos(\omega_p t)\\
\approx& \omega_b b^\dagger b - \frac{E_C}{12N^2}\left(b + b^\dagger\right)^4 + \frac{\delta E_J\omega_b}{4E_J}\left(b + b^\dagger\right)^2\cos(\omega_p t)
\end{aligned} \tag{S2}$$

Here, we have dropped the constant terms and set $\omega_b = \sqrt{8E_CE_J/N_0}$ for simplicity. When the conditions

$$\omega_p \gg \frac{E_C}{12N^2}, \qquad \text{and} \qquad \omega_p \gg \frac{\delta E_J\omega_b}{4E_J}, \tag{S3}$$

TABLE S1: Experimental device parameters for the parametrically pumped nonlinear oscillator in Ref. [S1].

Parameter	N	E_J	E_C	ω_p	$K/2\pi$	$P/2\pi$
Value	10	1.053 GHz	82.79 GHz	~ 16 GHz	17.3 MHz	~ 60 MHz

*xia-208@163.com

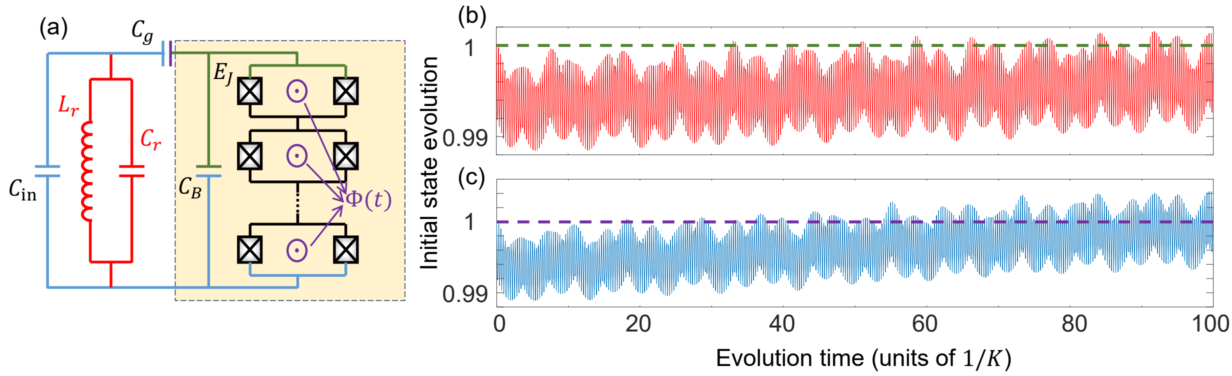

FIG. S1: (a) Circuit diagram of an array of Josephson junctions coupled to an LC resonator. The Josephson energy E_J is tunable by controlling the external magnetic flux $\Phi(t)$. The array of Josephson junctions with capacitance and Josephson energy C_J and E_J are shunted by an additional large capacitance C_B, matched by a comparably large gate capacitance C_g. The yellow-shaded area highlights the parametrically-driven Kerr-nonlinear resonator, which constructs the cat-state qubit. (b) Time evolution of the initial state $|\mathcal{C}_+^\beta\rangle$ governed by the effective Hamiltonian $H_{\rm KNR}$ (green-dashed curve) and the actual Hamiltonian $H_{\rm KNR}^{(0)}$ (red-solid curve). (c) Time evolution of the initial state $|\mathcal{C}_-^\beta\rangle$ governed by the effective Hamiltonian $H_{\rm KNR}$ (purple-dashed curve) and the actual Hamiltonian $H_{\rm KNR}^{(0)}$ (blue-solid curve). Parameters are listed in Table S1 and the numerical simulations are taken with the same rotating frame.

are satisfied, the counter-rotating terms in Eq. (S2) can be neglected under the rotating-wave approximation. The effective Hamiltonian reads

$$H_{\rm KNR}^{\rm eff} = \omega_c b^\dagger b - K b^{\dagger 2} b^2 + P b^{\dagger 2} \exp\left(-i\omega_p t\right) + P^* b^2 \exp\left(i\omega_p t\right), \tag{S4}$$

where the parameters are

$$K = \frac{E_C}{2N^2}, \qquad \omega_c = \omega_b - 2K, \qquad \text{and} \qquad P = \frac{\omega_b \delta E_J}{8E_J}. \tag{S5}$$

In the interaction picture, the Hamiltonian $H_{\rm KNR}^{\rm eff}$ becomes

$$H_{\rm KNR}^{\rm eff} = \Delta b^\dagger b - K b^{\dagger 2} b^2 + P b^{\dagger 2} + P^* b^2, \tag{S6}$$

which is the Hamiltonian describing a parametrically-driven Kerr-nonlinear resonator (KNR). Here $\Delta = \omega_c - \omega_p/2$ is the detuning.

Using the experimental parameters (see Table S1) reported in Ref. [S1], we give comparisons between the actual dynamics governed by $H_{\rm KNR}^{(0)}$ and the effective dynamics governed by $H_{\rm KNR}^{\rm eff}$ in Figs. S1(b) and S1(c). The actual dynamics coincides very well with the effective one (differences are less than 1%), indicating that the circuits in Fig. S1(a) can be well simplified to the KNR described by the Hamiltonian $H_{\rm KNR}^{\rm eff}$ in Eq. (S6). Moreover, Figs. S1(b) and S1(c) show that the system mostly remains in the initial state after a long-time evolution. This means that the initial states $|\mathcal{C}_\pm^\beta\rangle$ are eigenstates of the Hamiltonian $H_{\rm KNR}^{(0)}$ in a suitable rotating frame. Therefore, the superconducting circuits in Fig. S1(a) can be well described by the effective Hamiltonian under the rotating-wave approximation:

$$\begin{aligned} H =& H_0 + H_{\rm KNR} + H_{\rm int}, \\ H_0 =& \Delta a^\dagger a + \delta b^\dagger b, \\ H_{\rm KNR} =& -K b^{\dagger 2} b^2 + P b^{\dagger 2} + P^* b^2, \\ H_{\rm int} =& \lambda a b^\dagger + \lambda^* a^\dagger b, \end{aligned} \tag{S7}$$

which corresponds to the Hamiltonian in Eq. (1) of the main text.

Note that the Kerr-cat qubit in Fig. S1(a) is a flux-tunable device, which could be sensitive to $1/f$ noise. However, the Kerr-cat experiment [S2] showed a strong suppression of frequency fluctuations due to $1/f$ noise for the pumped cat, compared to when operating the Josephson-junctions array as a conventional transmon qubit without pumping.

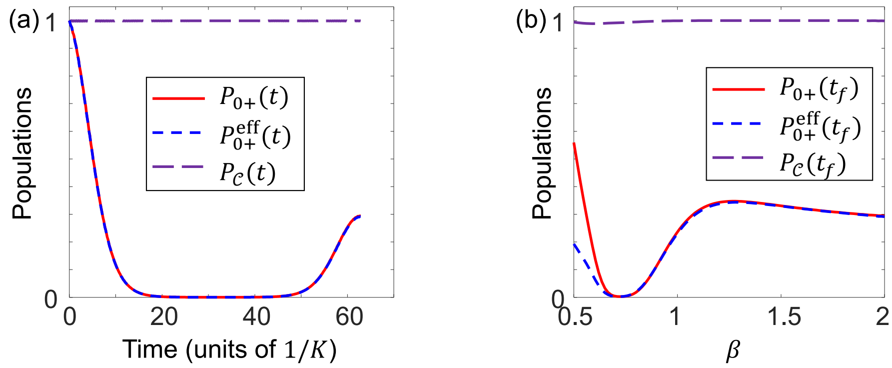

FIG. S2: (a) Time evolution of the initial state $|0,\mathcal{C}_+\rangle$ in the presence of single-photon loss in the KNR with $\kappa_b = 0.1\Delta$. (b) Populations of the state $|0,\mathcal{C}_+^\beta\rangle$ at time $t_f = 2\pi/g$ calculated for different β. The populations $P_{0+}(t) = \langle 0,\mathcal{C}_+^\beta|\rho(t)|0,\mathcal{C}_+^\beta\rangle$ and $P_{0+}^{\rm eff}(t) = \langle 0,\mathcal{C}_+^\beta|\rho_{\rm eff}(t)|0,\mathcal{C}_+^\beta\rangle$ are calculated using the master equations in Eq. (S10) and Eq. (S13), respectively. To focus on the influence of single-photon loss in the KNR, we assume $\kappa_a = \kappa_a^\phi = \kappa_b^\phi = 0$. Other parameters are $\lambda = \Delta = 0.1K$ and $\tilde{\delta} = 0.01\Delta$.

S2. SINGLE-PHOTON LOSS AND PURE DEPHASING

We consider two kinds of major noise: single-photon loss and pure dephasing. The system dynamics is described by the Lindblad master equation

$$\dot{\rho} = -i[H,\rho] + \sum_{j=a,b} \kappa_b \mathcal{D}[j]\rho + \kappa_j^\phi \mathcal{D}[j^\dagger j]\rho. \tag{S8}$$

In the Hamiltonian H, when the coupling strength λ is far small than the energy gap $E_{\rm gap} \simeq 4K|\beta|^2$, the dynamics of the KNR is well confined to the cat subspace $\mathcal{C}$. We can project the system onto the eigenstates of $H_{\rm KNR}$ with the projection operator:

$$P_{\rm KNR} = \sum_m |m\rangle\langle m| \otimes \sum_n |\psi_n\rangle\langle\psi_n|, \tag{S9}$$

where $|m\rangle$ are the Fock states of the cavity mode a and $|\psi_n\rangle$ are the eigenstates of $H_{\rm KNR}$ satisfying $H_{\rm KNR}|\psi_n\rangle = \xi_n|\psi_n\rangle$. Note that $|\psi_0\rangle = |\mathcal{C}_+^\beta\rangle$ and $|\psi_1\rangle = |\mathcal{C}_-^\beta\rangle$ are two degenerate eigenstates with $\xi_0 = \xi_1$. In the following, we independently analyze the influence of single-photon loss and pure dephasing on the system.

A. Single-photon loss

The influence of the single-photon loss in the KNR can described by:

$$\begin{aligned}\kappa_b\mathcal{D}[P_{\rm KNR} b P_{\rm KNR}]\rho \approx & \kappa_b|\beta|^2\mathcal{D}\left[\sqrt{\tanh|\beta|^2}|\mathcal{C}_+^\beta\rangle\langle\mathcal{C}_-^\beta| + \sqrt{\coth|\beta|^2}|\mathcal{C}_-^\beta\rangle\langle\mathcal{C}_+^\beta|\right]\rho \\ & +\kappa_b\mathcal{D}\left[\sqrt{\frac{\mathcal{N}_+}{\mathcal{N}_+^e}}|\mathcal{C}_+^\beta\rangle\langle\psi_2| + \sqrt{\frac{\mathcal{N}_-}{\mathcal{N}_-^e}}|\mathcal{C}_-^\beta\rangle\langle\psi_3|\right]\rho \\ & +\kappa_b|\beta|^2\mathcal{D}\left[\sqrt{\frac{\mathcal{N}_-^e}{\mathcal{N}_+^e}}|\psi_3\rangle\langle\psi_2| + \sqrt{\frac{\mathcal{N}_+^e}{\mathcal{N}_-^e}}|\psi_2\rangle\langle\psi_3|\right]\rho,\end{aligned} \tag{S10}$$

where $\mathcal{N}_+^e$ and $\mathcal{N}_+^e$ are normalization coefficients for the eigenstates $|\psi_2\rangle$ and $|\psi_3\rangle$, respectively. We have omitted highly excited eigenstates of the KNR because they are never excited in the presence of the single-photon loss.

According to the terms in red font in Eq. (S10), the single-photon loss can only lead to transition from the excited eigenstates $|\psi_{2,(3)}\rangle$ to the ground eigenstates $|\mathcal{C}_\pm^\beta\rangle$. If a KPO is initially in the cat-subspace $\mathcal{C}$, it always remains in this cat-subspace in the presence of single-photon loss. Figure S2(a) shows that the no-leakage probability (see the purple-dashed curve)

$$P_{\mathcal{C}} = \langle \mathcal{C}_+^\beta | \rho(t) | \mathcal{C}_+^\beta \rangle + \langle \mathcal{C}_-^\beta | \rho(t) | \mathcal{C}_-^\beta \rangle, \tag{S11}$$

mostly remains in 1 in the presence of single photon loss in the KNR. Therefore, we can neglect the terms in the last two lines in Eq. (S10) and obtain

$$\mathcal{D}[P_{\rm KNR} b P_{\rm KNR}]\rho \;\simeq\; \frac{|\beta|^2}{\sqrt{1-e^{-4|\beta|^2}}} \mathcal{D}[\sigma_x + i e^{-2|\beta|^2}\sigma_y]\rho. \tag{S12}$$

For large $|\beta|$, it can be simplified to $\mathcal{D}[P_{\rm KNR} b P_{\rm KNR}]\rho \simeq |\beta|^2 \mathcal{D}[\sigma_x]$. The master equation in Eq. (S10) is simplified to

$$\dot{\rho}_{\rm eff} = -i[H_R, \rho] + \kappa \mathcal{D}[a]\rho + +\kappa_a |\beta|^2 \mathcal{D}\left[\sigma_x\right]\rho + \kappa_a^\phi \mathcal{D}[a^\dagger a]\rho + \kappa_b^\phi \mathcal{D}[b^\dagger b]\rho. \tag{S13}$$

Assuming that the initial state is $|0, \mathcal{C}_+^\beta\rangle$, we show in Fig. S2(a) the actual dynamics with Eq. (S10) coincides very well with the effective dynamics with Eq. (S13). Figure S2(b) confirms that the effective master equation in Eq. (S13) is valid for large β, indicating the validity of the approximations.

B. Pure dephasing

The influence of pure dephasing can be described as:

$$\begin{aligned}
\kappa_b^\phi \mathcal{D}\left[P_{\rm KPO} b^\dagger b P_{\rm KPO}\right]\rho =& \kappa_b^\phi |\beta|^4 \mathcal{D}\left[\frac{\mathcal{N}_-}{\mathcal{N}_+} |\mathcal{C}_+^\beta\rangle\langle\mathcal{C}_+^\beta| + \frac{\mathcal{N}_+}{\mathcal{N}_-} |\mathcal{C}_-^\beta\rangle\langle\mathcal{C}_-^\beta|\right]\rho \\
&+ \kappa_b^\phi |\beta|^2 \mathcal{D}\left[\frac{\mathcal{N}_+}{\sqrt{\mathcal{N}_- \mathcal{N}_+^e}} |\psi_2\rangle\langle\mathcal{C}_-^\beta| + \frac{\mathcal{N}_-}{\sqrt{\mathcal{N}_+ \mathcal{N}_-^e}} |\psi_3\rangle\langle\mathcal{C}_+^\beta|\right]\rho \\
&+ \kappa_b^\phi |\beta|^4 \mathcal{D}\left[\frac{\mathcal{N}_-^e}{\mathcal{N}_+^e} |\psi_2\rangle\langle\psi_2| + \frac{\mathcal{N}_+^e}{\mathcal{N}_-^e} |\psi_3\rangle\langle\psi_3|\right]\rho.
\end{aligned} \tag{S14}$$

As in the above analysis, we have ignored the highly excited eigenstates of the KNR because they are mostly unexcited in the evolution. For large $|\beta|$, we have

$$\frac{\mathcal{N}_-}{\mathcal{N}_+} |\mathcal{C}_+^\beta\rangle\langle\mathcal{C}_+^\beta| + \frac{\mathcal{N}_+}{\mathcal{N}_-} |\mathcal{C}_-^\beta\rangle\langle\mathcal{C}_-^\beta| \simeq |\mathcal{C}_+^\beta\rangle\langle\mathcal{C}_+^\beta| + |\mathcal{C}_-^\beta\rangle\langle\mathcal{C}_-^\beta| = \mathbb{1}_\beta. \tag{S15}$$

That is, in the cat-state subspace, pure dephasing in KNR cannot cause significant infidelities. However, according to the terms in red font in Eq. (S14), pure dephasing can cause transitions from the cat states to the first-excited states $|\psi_{2,(3)}\rangle$ with a rate $\kappa_b^\phi |\beta|^2$.

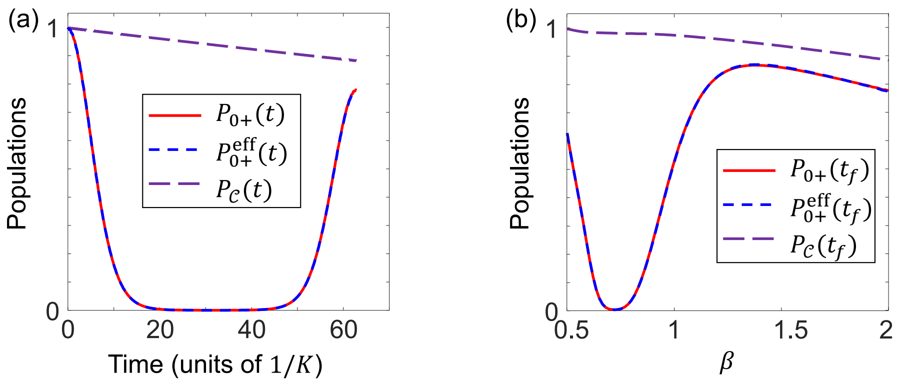

FIG. S3: (a) Time evolution of the initial state $|0, \mathcal{C}_+\rangle$ in the presence of pure dephasing in the KNR with $\kappa_b^\phi = 0.005\Delta$. (b) Populations of the initial state $|0, \mathcal{C}_+^\beta\rangle$ at time $t_f = 2\pi/g$ calculated for different β. To focus on the influence of pure dephasing in the KNR, we assume $\kappa_a = \kappa_a^\phi = \kappa_b = 0$. Other parameters are the same as those in Fig. S2.

Therefore, the master equation can be further simplified as

$$\dot{\rho}_{\text{eff}} = -i[H_R, \rho] + \kappa \mathcal{D}[a]\rho + +\kappa_a |\beta|^2 \mathcal{D}\left[\sigma_x\right]\rho + \kappa_a^\phi \mathcal{D}[a^\dagger a]\rho + \mathcal{L}\rho, \tag{S16}$$

where $\mathcal{L}\rho$ denotes the leakage term in Eq. (S14). We numerically demonstrate this approximation in Fig. S3. In the presence of pure dephasing, the populations (red-solid curves in Fig. S3), calculated using the master equation in Eq. (S8), are almost the same as those calculated using the effective one in Eq. (S16). Moreover, Fig. S3(b) shows that the leakage possibility increases when β increases, which is in agreement with the theoretical prediction in Eq. (S14).

C. Pair-cat qubit

Following the calculations from Eq. (S8) to Eq. (S16), we can analyze the influence of single-photon loss and pure dephasing for the pair-cat qubit. We first calculate the influence of single-photon losses. Note that it is difficult to obtain the exact eigenstates of the Hamiltonian H to construct a projection operator like P_{KNR} in the full Hilbert subspace. To calculate the influence of single-photon losses, we need to use the action of a on different states:

$$\begin{aligned} &a|0_\pm, \pm x\rangle = \pm\alpha|0_\pm, \pm x\rangle, \\ &a|1_\pm, \pm x\rangle = \left[D(\pm\alpha)|0\rangle \pm \alpha D(\pm\alpha)|1\rangle\right] \otimes \frac{1}{\sqrt{2}}\left(|\mathcal{C}_+^\beta\rangle \pm |\mathcal{C}_-^\beta\rangle\right) = |0_\pm, \pm x\rangle \pm \alpha|1_\pm, \pm x\rangle, \end{aligned} \tag{S17}$$

where $|n, \pm x\rangle$ are defined in Eq. (8) of the main text as

$$|n_\pm, \pm x\rangle \simeq D(\pm\alpha)|n\rangle \otimes \frac{1}{\sqrt{2}}\left(|\mathcal{C}_+^\beta\rangle \pm |\mathcal{C}_-^\beta\rangle\right), \tag{S18}$$

Note that we have assumed $\alpha = \alpha^*$ and $\beta = \beta^*$ for simplicity. Equation (S17) implies that the single-photon loss in the cavity a can only cause transition from the excited eigenstates $|1_\pm, \pm x\rangle$ to the ground eigenstate $|0_\pm, \pm x\rangle$. Therefore, considering together the result of Eq. (S10), when the system is initially in the computational subspace spanned by $|0_\pm, \pm x\rangle$, it always remains in this subspace in the presence of single-photon losses. Thus, we can obtain the effective Lindblad superoperator for single-photon losses in the pair-cat subspace $\mathcal{C}_\mu = \{|\mu_\pm\rangle\}$ as

$$P_\mu\left(\mathcal{D}[a]\rho + \mathcal{D}[b]\rho\right)P_\mu \approx \left(\alpha^2 + \beta^2\right)\mathcal{D}\left[|\mu_+\rangle\langle\mu_-| + |\mu_-\rangle\langle\mu_+|\right]\rho, \tag{S19}$$

which only describes bit-flip errors in the pair-cat qubit.

When analyzing the influence of pure dephasing, we first consider the dynamics in the pair-cat subspace $\mathcal{C}_\mu$ using the projection

$$P_\mu\left(\mathcal{D}[a^\dagger a]\rho + \mathcal{D}[b^\dagger b]\rho\right)P_\mu \approx \left(\alpha^4 + \beta^4\right)\mathcal{D}\left[|\mu_+\rangle\langle\mu_+| + |\mu_-\rangle\langle\mu_-|\right]\rho. \tag{S20}$$

This indicates that the pair-cat qubit is robust against phase-flip error. However, similar to the calculation in Eq. (S14), the actions of $a^\dagger a$ and $b^\dagger b$ on the states $|\mu_\pm\rangle$:

$$\begin{aligned} a^\dagger a|0_\pm, \pm x\rangle =& \alpha^2|0_\pm, \pm x\rangle \pm \alpha|1_\pm, \pm x\rangle, \\ b^\dagger b|0_\pm, \pm x\rangle \approx& \beta^2|0_\pm, \pm x\rangle \pm \beta|0_\pm\rangle \otimes \mathcal{D}[\pm\beta]|1\rangle, \end{aligned} \tag{S21}$$

can cause leakage out of the pair-cat subspace $\mathcal{C}_\mu$. To sum up, for our simulation protocol, pure dephasing should be as small as possible.

[S1] Z. Wang, M. Pechal, E. A. Wollack, P. Arrangoiz-Arriola, M. Gao, N. R. Lee, and A. H. Safavi-Naeini, Phys. Rev. X **9**, 021049 (2019), URL https://link.aps.org/doi/10.1103/PhysRevX.9.021049.
[S2] A. Grimm, N. E. Frattini, S. Puri, S. O. Mundhada, S. Touzard, M. Mirrahimi, S. M. Girvin, S. Shankar, and M. H. Devoret, Nature (London) **584**, 205 (2020), URL https://doi.org/10.1038/s41586-020-2587-z.
[S3] J. Koch, T. M. Yu, J. Gambetta, A. A. Houck, D. I. Schuster, J. Majer, A. Blais, M. H. Devoret, S. M. Girvin, and R. J. Schoelkopf, Phys. Rev. A **76**, 042319 (2007), URL https://link.aps.org/doi/10.1103/PhysRevA.76.042319.
[S4] J. Q. You, X. Hu, S. Ashhab, and F. Nori, Phys. Rev. B **75**, 140515(R) (2007), URL https://doi.org/10.1103/physrevb.75.140515.